Biomedical Signal Processing and Control 59 (2020) 101902

Contents lists available at ScienceDirect

Biomedical Signal Processing and Control

journal homepage: www.elsevier.com/locate/bspc

A new emotion detection algorithm using extracted features of the different time-series generated from ST intervals Poincaré map

Maryam Baghizadeh [a], Keivan Maghooli [a,*], Fardad Farokhi [b], Nader Jafarnia Dabanloo [a]

[a] Department of Biomedical Engineering, Science and Research Branch, Islamic Azad University, Tehran, Iran
[b] Department of Biomedical Engineering, Central Tehran Branch, Islamic Azad University, Tehran, Iran

ARTICLE INFO

Article history:
Received 30 September 2019
Received in revised form 30 January 2020
Accepted 15 February 2020

Keywords:
Electrocardiogram (ECG)
Emotion detection
Poincaré map
Feature extraction
Pan-Tompkins algorithm

ABSTRACT

Emotion recognition using biological signals plays an essential role in studying psychological states. In many studies, the distinct effect of each physiological signal usually is ignored. By limiting the physiological signals and just evaluating the ECG signals, the paper aims to study the dynamical behavior of the Poincaré map in the form of the feature extraction from the generated time-series. For this purpose, the detection of emotional states in the two-dimensional model of emotion (Arousal-Valence) is utilized using the electrocardiogram signals recorded on the MAHNOB-HCI tagging database. So after signal processing, the waves of Q, R, S, and T are detected by processing the ECG signals using the Pan-Tompkins algorithm. The Poincaré map is adopted for the RR, QT, and ST intervals, then five different time-series are extracted from this mapping, subsequently, various features are extracted from these different time-series in the time domain, frequency domain, time-frequency domain, and nonlinear domain analysis. Finally, the classification of emotional states is performed using three classifiers: KNN, SVM, and MLP. In this study, the extracted optimal features of the different time-series generated from Poincaré map of the ST Intervals are achieved the best average accuracies of 82.17 % ± 4.73 and 78.07 % ± 3.59 in the arousal and valence model, respectively. The superiority of the obtained results from the extracted features of the five different time-series generated from ST-Intervals Poincaré map expresses that in comparison with RR and QT Intervals, the ST Intervals are more affected by ANS response to the emotional stimuli.

1. Introduction

1.1. Importance and expression of the issue

A feeling is a complex physiological state that consists of three components: a mental experience, a physiological response, and a behavioral or meaningful response [1]. Emotion is described as the consistent separated responses to events (external or internal) for an organism [2]. Plutchik proposed eight basic emotional states: anger, fear, sadness, disgust, surprise, curiosity, pleasure and joy. The other emotional states can be made of the mixture of these basic emotions (For example, disappointment is a mixture of sadness and wonder) [3].

Ekman began his work on the relationship between facial expression and emotion from several fundamental global emotions: anger, hatred, fear, joy, sadness, and surprise [4]. In the other point of view, emotion is expressed in terms of Valence, Arousal, and Dominance dimensions (VAD). Valence from very positive emotion goes to very negative feelings (or unpleasant to pleasant); the Arousal (also called activation) range begins from the states of sleepiness up to excite, and finally, the Dominance is related to the strength of feelings [4,5]. The most common model for feelings is the circumplex model of emotion, which uses only the arousal and valence levels [6]. So far, comprehensive systems have not been developed to detect different emotional states due to different criteria of measurement. With the development of the field of human-computer interface (HCI), the emotion recognition research has been conducted.

Many previous studies have shown that physiological signals can reflect emotional changes [7–9]. These studies have indicated that the characteristics of physiological signals (more specifically, different types of used features in comparison with the number of used features) are played directly an important role in classification performance. In other words, the computational time of the detection algorithm to emotion recognition is another challenge in real-time applications. Feature extraction and feature selection are important steps since the optimal feature extraction can result in the improvement of classification and the evaluated indicators.

* Corresponding author.
E-mail address: k_maghooli@srbiau.ac.ir (K. Maghooli).

https://doi.org/10.1016/j.bspc.2020.101902
1746-8094/

The goal of researches is the emotional state detection system, which can provide optimum performance in terms of accuracy and response speed. Researches have shown that physiological signals are affected by emotion. However, in most of the studies, fusion of physiological signals is used for better detection; so that, the distinctive and accurate effects of emotion in each of these physiological signals are largely overlooked. However, the challenge that has been addressed recently is trying to focus on a smaller number of physiological signals to identify and review. The emotional state detection system can be designed in a user-dependent or user-independent manner [7–9]. The results of the studies have shown that user-dependent systems are achieved a higher level of accuracy than user-independent systems. Besides, methods of emotion detection are designed through analyzing the physiological signals generated by the autonomic nervous system (ANS). Physiological signals have the advantage that are immediately affected by emotional changes, which can not be routinely evaluated. Hence, many studies have concluded that the use of physiological signals is one of the most accurate ways to detect emotion.

Since physiological signals are non-linear and non-stationary, many studies have shown that the extracted features of the time-domain and frequency-domain are inappropriate for obtaining an intrinsic property of physiological signals. To identify emotion using physiological signals, choosing a proper set of features will be important.

Many studies have suggested several methods for feature extraction; one method extracts statistical features from the time domain, and another method such as Fourier transform is employed to extract features of the frequency domain. The fundamental issue in emotion detection systems is that, which one of the biological signals more often could reflect emotional states? Additionally, the responses of the subject may be different in the same emotional state. In this paper, we have tried to limit the biological signals and only evaluate the ECG signal to detect emotions. The general purpose of this paper is to analyze the dynamical behavior of the Poincaré map in the framework of the extraction of the different time-series from this mapping. For this purpose, various features of the different time series generated from the Poincaré map are extracted to identify emotion, and by selecting the most appropriate features, the emotion states have been more accurately detected. This paper is organized as below:

Section 2 is dedicated to explain the materials and methods. In section 3, you can see the results. Section 4 is for discussion, and finally, the paper is concluded in section 5.

1.2. Literature review

Considerable studies have been done to identify emotion in recent years. From a general point of view, a multiple categorization can be considered for the related studies: studies from the perspective of the database; the number of emotional states, the number of physiological signals, the extracted features and the used techniques to classify the desired emotional states.

Zheng et al. studied the EEG signals on the two databases of DEAP and SEED. The stimulation of emotion has been done through video clips, and in the study; positive, negative and neutral feelings have been investigated. The features such as the asymmetry (ASM), differential asymmetry (DASM), differential entropy (DE), power spectral density (PSD), rational asymmetry (RASM), and differential caudally (DCAU) have been extracted from the EEG signals, Also the dimension reduction has been accomplished through the PCA algorithm and the MRMR algorithm. Using the two classifiers SVM and GELM, accuracies of 69.67 % and 91.07 % have been achieved for the DEAP and SEED databases, respectively [10]. Becker et al. used the EEG signals on the HR-EEG database. In the study, an audio-visual stimulus has been used, and features such as the power of Alpha, Beta, Gamma and Theta bands, PSI in bands, HOC in bands and SPFs have been extracted, also the butter worth filter, T-test, dimension reduction of PCA and SVM classifier have been used. The results have shown that the HOC feature extraction from the frequency bands has yielded better results than the HOC feature extracted from the whole signals [11]. In the study by Subramanian et al., ASCERTAIN database and 36 films have been used to stimulate emotion, so that in this database, three emotional states and five personality states have been examined. Data preprocessing has been performed by the MATLAB Psych toolbox. The different features have been extracted including 10 features of the power spectrum density of low frequency, 4 features of the power spectrum density of the very slow response, Inter beat interval (IBI), Heart rate (HR), Heart Rate Variability (HRV). Identification of the most distinctive feature by LDA and validation by Mean F1-Score have been done, and finally, the two classifiers of NB and SVM have been used. The best results have reported by the NB classifier with an accuracy of 60 % for the arousal dimension and 59 % for the valence dimension [12]. Eleftheriadis et al. used the posed and spontaneous data from three available databases (CK+, Shoulder-pain, and DISFA). Then geometrical features of the different facial expressions and the apparent features of the histogram local binary pattern (LBP) have been extracted. The MC-LVM model has been proposed in the study, and finally, an average accuracy of 90.99 % has been reported [13]. Katsigiannis & Ramzan used the collected ECG signals on the DREAMER database. Emotional stimulation has been performed through audio-visual stimuli, and nine emotional states have been considered in the model of arousal and valence dimensions. The Pan-Tompkins algorithm has been used to detect the QRS complex. In the study, statistical features such as max, min, median, standard deviation, mean, and rang have been extracted through the Augsburg Bio-signal Toolbox, also, the features of HRV such as PSD for LF, PSD for HF, LF/HF ratio, total power, and RMSSD have been extracted via Vidaurre et al.'s BioSig toolbox. Finally, using the mean F1-score validation and SVM classification with the RBF kernel, the accuracy was reported 62.37 % for the valence level, 62.37 % for the arousal level and 61.57 % for dominance level [14]. Samara et al. used EEG signals collected on the DEAP database. statistical features such as mean standard deviation, mean of the absolute values of the first differences, mean of the normalized absolute values of the first differences, mean of the absolute values of the second differences, mean of the normalized absolute values of the second differences, power spectral density from brain waves and HOS have been extracted. In the study, SAM and Russell's circumplex model of emotion were evaluated and then, using the SVM classification, accuracies obtained for valence and arousal were reported 74.53 % and 68.15 % respectively [15]. In another study by Mangalagowri and Raj [16], EEG signals have been used for the detection of emotion (four types of emotional states), feature extraction has been done through DTW decomposition into 8 levels of frequency bands of alpha, beta, gamma, delta, theta, and finally classification has been implemented using feed-forward backpropagation algorithm. The feature classification has been performed by obtaining an accuracy of 75 % for normal patients and 65 % for abnormal patients. Kar et al. [17] used fuzzy features, SVM classification, and fuzzy rule to classify four types of emotion. The results of the study have reported that choosing the appropriate parameters from the kernel can increase the accuracy of over 30 %. In the study of Zhang et al., they used three databases of RML, eLTER-FACE05, and BAUM-15 to detect emotion by facial expressions. Finally, the three classifiers of CNN, 3D-CNN, and DBN have been used for classification [18]. Tzirakis et al. [19] used the RECOLA database with audio-visual channels, ECG and EDA signals, and classification of emotion have been done using appearance and geometric features and their combination in the two dimensional model of arousal-valence By the multimodal network. In the study of Perdiz et al. [20],

EMG signals of the face and EOG signals have been used to distinguish four types of emotion using facial expressions. Michalopoulos and Bourbakis used EEG signals collected on the DEAP database, and they used features of sample entropy and multi-scale entropy extracted from frequency bands of alpha and beta to detect emotion [21]. In the study of Gong et al., four emotional states have been classified through the ECG, RSP, EMG and SC signals. In the study, the features of the time domain, time-frequency, non-linear, and intrinsic mode functions have been extracted. Finally, using the decision tree classifier of C4.5, the best accuracy has been obtained by the fusion of the attributes; also, the results of the study have shown that IMF features have a better performance than the other features [22]. Scherz et al. [23] showed the distinction between physical activity and stress using RR Intervals. In the other study by Scherz et al. [24], the distinction between stress and physical activity have been studied using a portable ECG/EMG system. They designed an experiment consisting of four stages of rest, physical activity, psychological stressors, and relaxation. ECG, EMG, and accelerometer have been recorded via wireless sensor nodes. ECG data have been evaluated by extracting the R peak of the QRS complex. The results have shown that in the resting stage, there are no changes in the signal; in comparison to the physical activity stage, in the temporary evolution of RR Intervals, there is a remarkable shift in the signal. Finally, using this shift, they examined the distinction between physical activity and stress. Ben and Lachiri [25] used the physiological signals on the MAHNOB-HCI database; by considering the nine emotional states and the extraction of the characteristics of the HRV signal and the mean RR intervals, the classification of emotion has been performed through SVM classifier with four different kernels. In a study by Moharreri et al., emotional states in the two-dimensional model of arousal and valence have been detected using triangle fuzzy space mapping (TPMS). In the study, the SAM evaluation model and the Kruskal-Wallis test have been used. The results have indicated that cold color is associated with low arousal and warm color is associated with high arousal [26]. In the study by Dabanloo et al. [27], using color stimulation, the emotional states have been considered in the two groups of pleasant and unpleasant. In the study, the analysis of HRV and distribution of points of the Poincaré plot of RR Interval has been used. Finally, by extraction of the features of phase space points, COM and GOM. Using the two tests of SAM, Kruskal-Wallis, and P-value. The results have shown that cool colors are associated with high levels of valence and warm colors are associated with low levels. Besides, in the study by Rezaei et al. [28], they used two groups of pictures stimuli. In the study, the HRV triangle indicator has been used; and then the features have been extracted in the domain of time, frequency, and analysis of the Poincaré domain. The results have indicated that HRV parameters can capture significant changes in ANS response to pictures stimuli. Ferdinando et al. used the ECG signals collected on the MAHNOB-HCI database to detect emotion in the arousal-valence model. For the study, the Pan-Tompkins algorithm for R peak-detection and BEMD analysis have been used to extract the features of IMFs in time domain and frequency domain; finally, using the KNN classifier (10-fold cross-validation), the accuracies of 55.8 % and 59.7 % have been reported for arousal and valence, respectively [29].

In most studies, the criterion of precision, sensitivity, and specificity have been used to show the classification results of class labels for the validation of classification techniques. In this study, we proposed a new algorithm for emotion detection in the AV model using only one of the biological signals (ECG) and subsequently, studied the nature of the hidden time-series in the Poincaré map.

1.3. Methodology and presentation structure

In this paper, the twelve steps algorithm of emotion detection is proposed for the classifying different emotional states in the two-class problem of the arousal and valence model. The block diagram of the emotion detection algorithm is shown in Fig. 1.

In this section, each of the steps of the proposed algorithm is briefly described: Firstly, the recorded ECG signals are collected from the database. In the second stage, three algorithms of data pre-processing are used to eliminate noise and artifacts from ECG signals. In the third step, the windowing of 1-minute is used as the window size for the signals. In the fourth step, signal processing is performed through the Pan-Tompkins algorithm, and the next step; RR, QT, and ST intervals are obtained after detecting the waves of the ECG signal. In the sixth step, the Poincaré map is adopted for each of the intervals, and in the seventh step, the five different time series are extracted from the Poincaré maps. In the eighth step, various features are extracted from each of the obtained time series from Poincaré map of RR, QT and ST intervals, in the time domain, frequency domain, time-frequency domain, and nonlinear domain analysis. In the ninth step, the normalization of the set of features is achieved. In the tenth step, the genetic algorithm is used to select the optimal features, and in the eleventh step; the p-value criterion is used for dimension reduction of the selected feature set. Finally, in the final stage, three classifiers of the K-nearest neighbor, support vector machine, and multi-layer perceptron neural network are used to classify different emotional states in the two-class problem of the arousal-valence model. Then, the results of this study are compared with other studies and the optimal method is presented with the best results. The structure of the presentation of the concepts of the paper will be as follows:

The section of techniques and methods is presented by data collection, database introduction, data preprocessing and signal processing, Poincaré map, the extracted five different time-series from Poincaré map, the extracted features from the five different time-series and classification structure. In the results section, average-accuracy, sensitivity, and specificity are achieved through the mentioned classifiers, and subsequently, the achieved results are compared together. Finally, in the section of discussion and the conclusion, from between intervals of RR, QT & ST, the optimal interval will be introduced. So that Poincaré map of this interval includes the hidden best information in response to the emotional stimuli. The results of this paper are compared with other studies and a set of suggestions for future studies will be presented.

2. Materials and methods

2.1. The data collection and data preprocessing

Soleymani et al. [30] have created the MAHNOB-HCI multimodal database, they have recorded physiological environmental signals of 30 participants (17 women and 13 men); they have considered nine emotional states by stimulating the emotion of individuals via the emotional films. In this database, the recorded physiological signals are including ECG, GSR, Temp and RESP signals; also, the EEG signals, eye gaze, and facial expressions have been recorded on the database. The participants' response files have included 47 channels and 30 s before and after each trial. In this paper, the 513-recorded ECG signals with a sampling frequency rate of 256 Hz were used on the MAHNOB-HCI database. In this database, ECG signals were collected in three channels of 33, 34, and 35; in this study, only the recorded ECG signals of the 35th channel were used. The ECG signals have been stored using Bio-semi data format (BDF) which are readable by EEGLAB. Finally, all files were converted to MAT format and implementation of this proposed algorithm was done by MATLAB software.

Fig. 1. Block diagram of the proposed emotion detection algorithm based on the ECG signal.

Table 1
Categorization of emotion in the Arousal-Valence model (two-class problem).

Arousal	Valence
high	negative
low	positive

Data preprocessing is an important step in identifying systems. ECG signals are included noises that can be arisen from frequency interference, baseline drift, electrode contact noise, polarization noise, and muscle noise, the internal amplifier noise and motor artifacts [31].

For this purpose, in this study, for the data preprocessing, three filters were used including IIR-notch filters, wavelet filter banks, and moving averaging filter (smoothing). The notch filter is used to remove power line interference. The wavelet filter bank (d4, which is compatible with vital signals) is used to eliminating and reducing the high-frequency components, this filter can also lead to the adjustment of the baseline. The level of decomposition is five levels, and the signal smoothing was performed using smoothness, which is used to remove motion artifacts from the ECG signals. The default coefficients of MATLAB software were also used to achieve the goal. According to Table 1, in this paper, the two-class problem is defined using the nine emotional keywords in arousal-valence model that these emotional keywords are as follows:

1) sadness, 2) joy, happiness; 3) disgust; 4) neutral; 5) amusement; 6) anger; 7) fear; 8) surprise; and 9) anxiety.

2.2. One-minute ECG signal

According to one of the studies [32], the physiological variability distribution of 1 min is widely used. So, 1 min time interval of ECG signals was achieved using 1-min window sizes for the classification of emotion in AV model; Hence in this study, the pre-processed ECG signal was segmented into a series of one-minute windows for extraction of Q, R, S, and T waves.

2.3. Data processing

Because of acquisition of high accuracy in detection of ECG peaks and data processing, the Pan-Tompkins algorithm [33] was used to detect the waves of Q, R, S, and T. The algorithm consists of five steps: a band-pass filter, a derivative operator, a squaring operation, moving integrator, and an adaptive threshold. By using this algorithm, the occurrence time and amplitude of all waves were obtained. Then, RR, QT and ST intervals were obtained by calculating the time difference between the two waves; R–R, Q–T, and S–T in the ECG signal.

In this paper, the ECG signals with Q, R, S and T waves have been segmented into a series of successive 1-min windows. A schematic of the ECG signal is shown in Fig. 2 for two heart cycles along with RR, QT, and ST intervals [34]. In the ECG signal, the most useful of clinical information is stored at the defined waves and intervals. The values of amplitude and duration for a normal ECG signal are presented in Table 2.

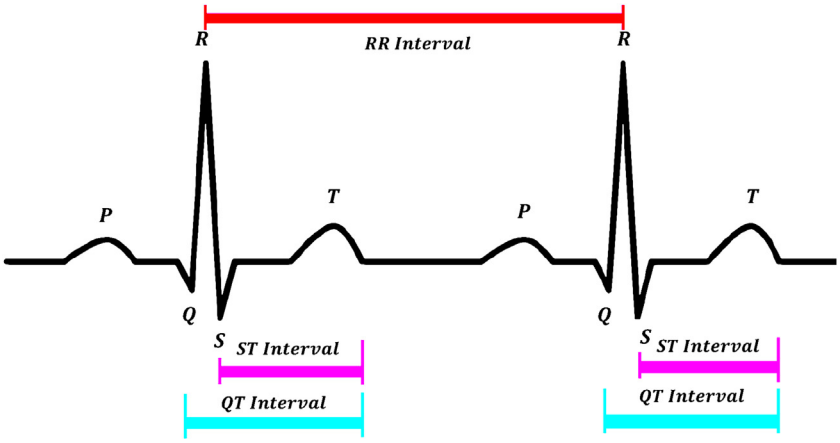

Fig. 2. Schematic of ECG signal; the defined waves; RR, QT, and ST Intervals [34].

Table 2
The amplitude and duration values for a normal ECG signal.

Amplitude	Duration
R-wave : 1.60 mV	Q-T interval : 0.35 to 0.44 s
Q-wave : 25 % R-wave	S–T interval : 0.05 to 0.15 s
T-wave : 0.1 to 0.5 mV	QRS interval : 0.09 s

2.4. Poincaré map

The analysis of the Poincaré map is a nonlinear method for detecting hidden patterns in a time series. On the other hand, Poincaré analysis is a quantitative method, in the sense that the Poincaré plot has several parameters that are called standard descriptors for quantifying visual information in the plot.

In previous studies, Poincaré plots have been shown as the obvious patterns of heart rate dynamics due to nonlinear processes. Since the SD1 and SD2 parameters cannot correctly represent the dynamics of Poincaré map, as the main objective of this study, the dynamics of the Poincaré map is investigated using the generated different time series from this map. Some of the extracted time series from the Poincaré map can be represented changes in the dynamics of ECG signals with higher accuracy [28]. The Poincaré map is a used technique for nonlinear dynamics and it is depicted for the nature of RR interval fluctuations. It is plotted in each R-R interval as a function of the previous R-R interval. The analysis of the Poincaré map is a quantitative-visual technique, which is categorized into functional classes by the form of the plot, and it has indicated the degree of heart failure in one person [35]. This plot provides a summary of information such as information details of the beat to beat in heart behavior [36]. The Poincaré map can be quantitatively analyzed by calculating the standard deviation of the R-R Intervals with lines of y = x, and $y = -x + 2R - R_m$, where $R - R_m$ is the mean of all of R-R Intervals [37].

Standard deviations are specified as SD1 and SD2, respectively. The SD1 is related to fast changes of beats in the data, while SD2 describes the long-term variations of R-R Interval [37]. The ratio of SD1 to SD2 (SD1/SD2) is also calculated to describe the relationship between details [38]. SD1/SD2 shows the ratio of short-term distance variations to long-term distance variations [38]. In this paper, three-time intervals of RR, QT, and ST were obtained after extracting Q, R, S, and T waves through the Pan-Tompkins algorithm. And then for the RR, QT and ST intervals; the Poincaré map was obtained based on the plotting of samples of RR(n), QT(n) and ST(n) versus RR(n+1), QT(n+1) and ST(n+1). In Fig. 3, the sample of Poincaré maps are depicted for the three intervals of RR, QT and ST extracted from the ECG signal.

2.5. The 5-different time-series extracted from Poincaré map

After plotting Poincaré map for RR, QT, and ST intervals, five different time-series were extracted from each of the mappings. 1) time series of distance in polar coordinate; 2) time series of angle in polar coordinate, 3) time series of shortest distance to 45° line; 4) time series of triangle area created by three consecutive vectors and 5) time series of angle between two consecutive vectors.

2.5.1. Time series of distance obtained from polar coordinate

To extracting various time series from the Poincaré map, initially, the polar coordinate in this mapping is applied and the r vector was obtained based on Eq. (1). For example, in Fig. 5(a) r_1, r_2 and r_3 vectors are depicted for three different points in the Poincaré map of RR Interval. According to Eq. (1), the distance of each point to the origin of the coordinate is calculated by using the root of the sum of squares of RR (n) and RR (n-1).

So according to Eq. (2), the distance time series in Poincaré map was obtained by sequences of the obtained distances in the Poincaré map of RR, QT and ST Intervals.

$$r_n = \sqrt{RR_n^2 + RR_{n-1}^2} \tag{1}$$

$$r_N = \{r_1,\ r_2,\ r_3,\ \ldots,\ r_n\} \tag{2}$$

2.5.2. Time series of angle obtained from polar coordinate

In addition to the distance of the points in polar coordinate, the angle (theta) between the points and the horizontal axis is obtained by mapping the Poincaré space to the polar coordinate. According to Eq. (3), the angle is calculated through the inverse tangent of $RR(n-1)$ to $RR(n)$ in polar coordinate. For example; in Fig. 5(b), the angles of θ_1, θ_2, and θ_3 are depicted for three different points in the Poincaré map of RR Interval.

Thus, according to Eq. (4), the angle time series in Poincaré map was obtained by sequences of the obtained angles in the Poincaré map of RR, QT and ST Intervals.

$$\theta_n = \tan^{-1}\frac{RR_{n-1}}{RR_n} \tag{3}$$

$$\theta_N = \{\theta_1,\ \theta_2,\ \theta_3,\ \ldots,\ \theta_n\} \tag{4}$$

2.5.3. Time series of shortest distance to 45° line

Every point on the Poincaré map has a distance to 45° line; however, the shortest distance can be evaluated as the vertical distance from the hypothetical point to the 45° line. The shortest distance to the 45° line can provide valuable information about the dynamics

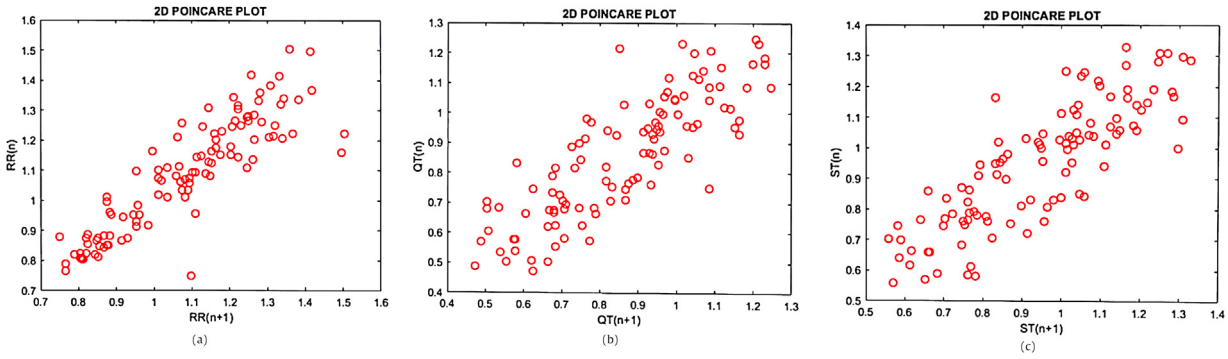

Fig. 3. Samples of Poincaré map are depicted for the three intervals obtained from the ECG signal; (a) RR Intervals Poincaré map, (b) QT Intervals Poincaré map, (c) ST Intervals Poincaré map.

of the signals if the distance was shorter, so it can show HRV signal reduction [39].

the shortest distance to the 45° line is depicted in Fig. 5(c) for several points above and below the 45° line (the distances above 45° line (D^1_{up}, D^2_{up} & D^3_{up}) and the distances below 45° line (D^1_{down} & D^2_{down})).

In Eq. (5), D_n is the shortest distance of the nth sample to the 45° line. R_{n+1} is the R-R Interval at the $n+1th$ sample; R_n is the R-R Interval at the nth sample [39].

Thus, according to Eq. (6), the time series of shortest distance to the 45° line was created by the sequence of obtained distances to the identify line of Poincaré map of the RR, QT, and ST Intervals.

$$D_n = \frac{\left|RR_{n+1} - RR_n\right|}{\sqrt{2}} \tag{5}$$

$$D_N = \{D_1,\ D_2,\ D_3,\ \ldots,\ D_n\} \tag{6}$$

2.5.4. Time series of triangle area created by three successive points

A triangle is created from three consecutive vectors, as it is shown in Fig. 5(d). To construct a triangle, the following process is performed:

Firstly, the point $(R_1,\ R_2)$ is connected to $(R_2,\ R_3)$. Secondly, the point $(R_2,\ R_3)$ is connected to $(R_3,\ R_4)$ and finally, the point $(R_3,\ R_4)$ is connected to $(R_1,\ R_2)$ [39]. The Eq. (7) is introduced to calculate the i th area of triangle [39]. In Eq. (7), A_i is the area of the ith triangle, R_i is the RR Interval at the ith sample, R_{i+1} is the RR Interval at the $i+1th$ sample, R_{i+2} is the RR Interval at the $i+2th$ sample, R_{i+3} is the RR Interval at the $i+3$th sample [39]. Therefore, four variables are required to calculate the area of a triangle [39]. For example, in Fig. 5(d), the created triangle area is plotted using three consecutive vectors. Thus, according to Eq. (8), the time series of triangle area was obtained using the sequence of the created triangle regions by three consecutive vectors in the Poincaré map of the RR, QT and ST Intervals.

$$A_i = \frac{1}{2}\left|det\begin{bmatrix} R_i & R_{i+1} & R_{i+2} \\ R_{i+1} & R_{i+2} & R_{i+3} \\ 1 & 1 & 1 \end{bmatrix}\right| = \frac{1}{2}\left|R_i\left(R_{i+2} - R_{i+3}\right) - R_{i+1}\left(R_{i+1} - R_{i+3}\right) + R_{i+2}\left(R_{i+1} - R_{i+2}\right)\right| \tag{7}$$

$$A_I = \{A_1,\ A_2,\ A_3,\ \ldots,\ A_i\} \tag{8}$$

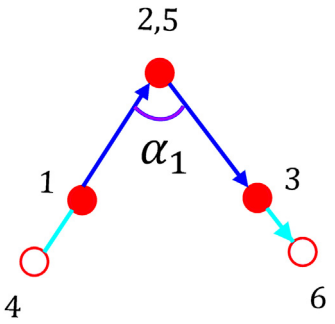

Fig. 4. Angle between vectors 1-2 & 2-3 is similar as the vectors 4-5 & 5-6 nevertheless, the length of vectors 1-2 & 3-4 is different from the vectors 4-5 & 5-6 [39].

2.5.5. Time series of angle between two consecutive vectors

To show some of the characteristics of the time series extracted from the Poincaré map, the angle between the successive vectors is used, so that it is constructed in Fig. 4 [39].

This angle can show better information about the spatial dynamics of the signals which are extracted over time [39]. In Eq. (9), it can be shown how the angle between two vectors is calculated. In the Eq. (9), α_i is ith angle; R_i is the RR Interval at the ith sample; R_{i+1} is the RR Interval at the $i+1$th sample and R_{i+2} is the RR Interval in the $i+2$th sample. According to Fig. 4, by using two vectors of 1–2 and 2–3; the first angle (α_1) is calculated by defining the 1st, 2th and 3th R-R Interval [39]. Fig. 5(e) provides a better knowledge about how of creating vectors and angles [39]. Thus, according to Eq. (10), the time series of angles between two consecutive vectors were obtained based on the sequence of the obtained angles between two successive vectors in the Poincaré map of the RR, QT and ST Intervals.

$$\alpha_i = \cos^{-1}\frac{R_iR_{i+1} + R_{i+1}R_{i+2}}{\sqrt{R_i^2 + R_{i+1}^2} + \sqrt{R_{i+1}^2 + R_{i+2}^2}} \tag{9}$$

$$\alpha_I = \{\alpha_1,\ \alpha_2,\ \alpha_3,\ \ldots.,\ \alpha_i\} \tag{10}$$

The five different time-series are summarized in Table 3, which have been extracted from each of the Poincaré map of RR, QT, and ST Intervals.

2.6. Feature extraction

At this stage, after obtaining the five different time-series from the Poincaré map of RR, QT & ST Intervals, different features were extracted in the time domain, frequency domain, time-frequency domain, and nonlinear domain analysis.

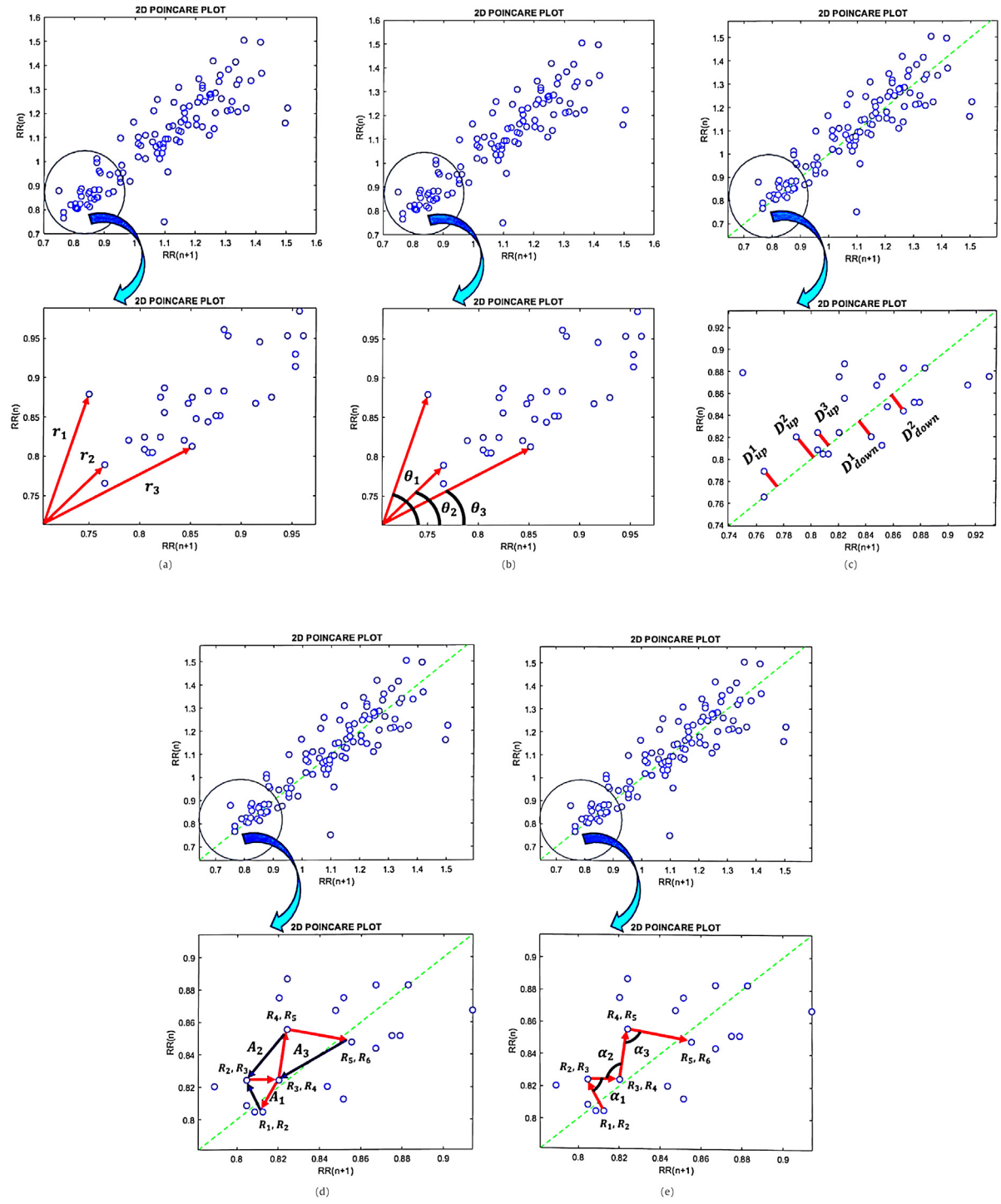

Fig. 5. The sample of schematic of the different time series generated from Poincaré map for RR Intervals; (a) Distance in polar coordinate, (b) Angle in polar coordinate, (c) Shortest distance to 45° line, (d) triangle area created by three consecutive vectors, (e) angle between two consecutive vectors.

Table 3
The 5-different Time-series extracted from the Poincaré map of RR, QT & ST intervals.

#	The extracted time-series	Equation (by considering RR, QT & ST = X)
1	r_N = Distance in polar coordinate	$r_n = \sqrt{X_n^2 + X_{n-1}^2}$
2	θ_N = Angle in polar coordinate	$\theta_n = \tan^{-1}\frac{X_{n-1}}{X_n}$
3	D_N = Shortest distance to 45° line	$D_n = \frac{\lvert X_{n+1} - X_n \rvert}{\sqrt{2}}$
4	A_I = Triangle area created by three consecutive vectors	$A_i = \frac{1}{2}\left\lvert det \begin{bmatrix} X_i & X_{i+1} & X_{i+2} \\ X_{i+1} & X_{i+2} & X_{i+3} \\ 1 & 1 & 1 \end{bmatrix}\right\rvert$
5	α_I = Angle between two consecutive vectors	$\alpha_i = \cos^{-1}\frac{X_iX_{i+1}+X_{i+1}X_{i+2}}{\sqrt{X_i^2+X_{i+1}^2}+\sqrt{X_{i+1}^2+X_{i+2}^2}}$

Table 4
The extracted features of the 5-different time-series obtained from Poincaré maps in the time domain.
AnalysisParameterDescriptionEquationTime DomainMax, MinMaximum or minimum sample in a time series._MeanAverage of all samples in a time series._VarianceIt is a measurement of the spread between samples in a time series around the mean of data._MADThe mean absolute deviation of a data set is the average distance between each data value () and the mean of data values.Where is the mean of the values , defined as:; is the total number of all in the segment.KurtosisKurtosis is a measure of the height and sharpness of the peak relative to the rest of the data._SkewnessSkewness is a measure of lack of symmetry of distribution, of the data._Diff_(XI)2Square successive difference of intervals (between each of the data samples () and its adjacent sample ()).SDNNThe standard deviation of the NN intervals of a time series.RMSSDThe root mean square successive difference of intervals.SDSDStandard deviation of differences between adjacent NN distances in a time series.Where is described by the following equation:

Analysis	Parameter	Description	Equation
Time Domain	Max, Min	Maximum or minimum sample in a time series.	-
	Mean	Average of all samples in a time series.	-
	Variance	It is a measurement of the spread between samples in a time series around the mean of data.	-
	MAD	The mean absolute deviation of a data set is the average distance between each data value (X_i) and the mean of data values.	$MAD\_XI = \frac{1}{N}\sum_{i=1}^{N}\lvert X_i - \overline{X}\rvert$ Where $\overline{X}$ is the mean of the values X_i, defined as: $\overline{X} = \frac{1}{N}\sum_{i=1}^{N} X_i$; N is the total number of all XI in the segment.
	Kurtosis	Kurtosis is a measure of the height and sharpness of the peak relative to the rest of the data.	-
	Skewness	Skewness is a measure of lack of symmetry of distribution, of the data.	-
	Diff_(XI)^2	Square successive difference of intervals (between each of the data samples (X_i) and its adjacent sample (X_{i-1})).	$Diff(XI)^2 = (\lvert X_i - X_{i-1}\rvert)^2$
	SDNN	The standard deviation of the NN intervals of a time series.	$SDNN = \sqrt{\frac{1}{N}\sum_{i=1}^{N}(X_i - \overline{X})}$
	RMSSD	The root mean square successive difference of intervals.	$RMSSD = \sqrt{\frac{1}{N-1}\sum_{i=1}^{N-1}(X_{i+1} - X_i)^2}$
	SDSD	Standard deviation of differences between adjacent NN distances in a time series.	$SDSD = \sqrt{\frac{1}{N-1}\sum_{i=1}^{N-1}(\lvert X_i - X_{i+1}\rvert - \overline{Xdif})^2}$ Where $\overline{Xdif}$ is described by the following equation: $\overline{Xdif} = \frac{1}{N-1}\sum_{i=1}^{N-1}(\lvert X_i - X_{i+1}\rvert)$

2.6.1. The feature extraction in time domain analysis

All features of the time domain are reflected in the various aspects of the statistical variability during time series distances. It can be shown that the variability is derived from the differences between adjacent internal distances. The statistical features that can be mentioned maximum (Max), minimum (Min), mean, variance (Var), mean absolute deviation (MAD), statistical features of kurtosis and skewness, and square successive difference of intervals (Diff_(XI)^2), Also; the parameters such as SDNN, SDSD and RMSS were extracted. So, these statistical parameters were extracted from the five different time-series with considering the adjacent intervals of a time series. For this purpose, by considering samples of the time series, the statistical parameters were calculated based on one sample (X_i) and its previous sample (X_{i-1}).

2.6.2. The feature extraction in frequency domain analysis

In terms of computational, the features of the time domain are obtained simpler than the frequency domain features. In this paper, the frequency domain features such as the Pcov, Pmcov, Pwelch, and periodogram methods were extracted to estimating the PSD method for each of the 5-different time-series obtained from Poincaré map. By specifying a sequence of data $X(n), 0 \leq n \leq N-1$; the parameters of this method are estimated [38].

Then, the density of the power spectrum is estimated by these parameters; but these methods suffer from spectral leakage effects due to windowing; Spectral leakage can lead to masking the weak signal that exists in the data [38].

2.6.3. The feature extraction in time-frequency domain analysis

The wavelet transform (WT) is a mathematical tool for signal analysis; In DWT, The signal is decomposed to approximation coefficients and detail coefficients [40].

In this study, the extracted features of these methods are reported in Table 5. Moreover, in the time-frequency analysis, the parametric methods can be lead to a higher frequency and time resolution. One of the parametric methods is the Autoregressive (AR) model [41].

The methods of estimating the parametric power spectrum (based on the model) prevent the leakage problem and these methods can be provided a better frequency resolution than the classical or non-parametric methods [38]. Moreover, time series can be modeled; AR and Burg methods can be used for the analysis of the time-frequency domain. In the AR method, the order of the AR model p = 16 can be taken [41]. Also, the Burg method is obtained in high resolution and it leads to a stable AR model [38].

2.6.4. The feature extraction in nonlinear domain analysis

Recent developments in nonlinear dynamics theory provide a way to analyze the generated signals from nonlinear biological systems. Now generally, it has been recognized that these nonlinear techniques can more effectively describe the processes produced by biological systems [38].

The extracted nonlinear features of the obtained five different time-series from Poincaré map of RR, QT & ST Intervals that can be mentioned, including as the following parameters:

The correlation dimension (CD), the largest Lyapunov exponent (LLE), approximate entropy (ApEn), sample entropy (SampEn), fuzzy entropy (Fuzzy En), Hurst exponent, fractal dimension (FD), detrended fluctuation analysis (DFA), Shannon entropy (Shannon En) and Kolmogorov Sinai entropy. In Tables 4–7, there are four categories of features: the time domain, frequency domain, time-frequency domain, and nonlinear domain analysis. In the tables, the equations and a brief description of parameters are presented; so that these parameters have been extracted from the five different time-series obtained from the Poincaré map of RR, QT, and ST Intervals.

Table 5
The extracted features of the 5-different time-series obtained from Poincaré maps in the frequency domain.

Analysis	Parameter	Description	Equation
Frequency Domain	Periodogram	It is an estimate of the spectral density of a signal.	-
	Pwelch	PSD is estimated using the welch method.	-
	Pcov	PSD is estimated using the covariance method.	-
	Pmcov	PSD is estimated using the modified covariance method.	-

Table 6
The extracted features of the 5-different time-series obtained from Poincaré maps in the time-frequency domain.

Analysis	Parameter	Description	Equation
Time-Frequency Domain	Mean, Variance, skewness, standard deviation (Std), MAD, Diff_(XI)^2	These are extracted from both the detail and approximation coefficients in the DWT (d4) with 5 decomposition levels (detail coefficients (d1, d2, d3, d4, d5) and approximation coefficient (a1)).	-
	Energy, Variance, Standard Deviation, and Waveform Length	The Multi-scale Wavelet Transform features are extracted by assuming 10 decomposition levels.	-
	AR model	The data of a time series are modeled as the output of a causal, all-pole, and discrete filter, which its input is a white noise ($w(n)$); the coefficients of the model are considered as a feature [38].	$x(n) = -\sum_{k=1}^{p} a(k)x(n-k) + w(n)$ Where $a(k)$ are coefficients of AR.
	Burg model	To obtain parameters of the AR model is used. $\hat{\vec{E}}$ is the least squared error. The Burg method is obtained at a high resolution and results in a stable AR model [38].	$P_{xx}^{BU}(f) = \frac{\hat{\vec{E}}_p}{\left\|1 + \sum_{k=1}^{p} \hat{a}_p(k)e^{-j2\pi fk}\right\|^2}$ Where $P_{xx}^{BU}(f)$ is the power spectrum of pth order of AR.

Table 7
The extracted features of the 5-different time-series obtained from Poincaré maps in the nonlinear domain.

Analysis	Parameter	Description	Equation
Nonlinear Domain	CD	It is used as a method for measuring the fractal dimension.	$CD = \lim_{r\to 0} \frac{\log(C(r))}{\log(r)}$ Where $C(r)$ is a correlation function; More details in [38].
	DFA	The root-mean-square fluctuation is measured from the integrated and detrended time series at different observation windows and it is plotted against the size of the observation window on a log-log scale [38].	$1F(n) = \sqrt{1/N\sum_{k=1}^{N}[y(k) - y_n(k)]^2}$ Where $y(k)$ is a time series, and $y_n(k)$ is the integrated and detrended series.
	Shannon En	It is a measure of the average content of information that is missing when it does not know the value of the random variable. If p denotes the probability density function of x, then entropy can be written as:	$H(X) = -\sum_{i=1}^{n} p(x_i)\,.\log_b p(x_i)$
	Fuzzy En	This parameter is calculated for fuzzy information measurements of time series.	-
	ApEn	It is a measure of system complexity. More details in [38].	$\mathrm{ApEn}(\mathrm{r},\ \mathrm{m}) = \ln\left[\frac{C^m(r)}{C^{m+1}(r)}\right]$ Where r and m are input parameters.
	SampEn	It measures the order of complexity of the time series. For more details about the equation, refer to [38].	$SampEn(m,\ r,\ N) = -\ln\left[\frac{\emptyset'^m(r)}{\emptyset'^{m+1}(r)}\right]$
	LLE	The largest Lyapunov exponent (λ) is defined as the average rate of divergence of the two neighboring trajectories [38].	$\lambda = \lim_{t\to\infty} \frac{1}{t}\ln\frac{\lvert\Delta x(x_0,\,t)\rvert}{\lvert\Delta x\rvert}$, More details in [38].
	Hurst exponent	It is used to evaluate the existence and absence of long-range dependence. It is used for the smoothness of a fractal time series [38]. It is defined as:	$H = \log(\frac{R}{S})/\log T$; Where T is the data sample duration, and $\frac{R}{S}$ is the corresponding value of the rescaled range.
	FD	Fractal dimension is a measure of roughness for time series [42]. In this study, it is computed by the box-counting method.	-
	Kolmogorov Sinai entropy	This entropy is a metric invariant of the dynamical system. For more details about the equation, refer to [43].	$h_q = \sup_{\mathcal{P}} \lim_{m\to\infty} h_q(m,\ \mathcal{P}_\varepsilon)$ Where h_q are the order-q of entropies.

Table 8
The method of feature selection.

Genetic algorithm
Step 1: the input Attribute Matrix formation. Step 2: Primary Populations Generation: To generate the population, several binary chromosomes with the number of genes equal to the number of attributes create randomly. Step 3: The fitness function is determined by increasing the accuracy of the AdaBoost algorithm. Step 4: Due to the rate of fitness function of each chromosome, a new population is created: A) Intersection: The two-parent chromosomes are intersected by the XOR function and the new population is created. B) Mutation: A random number is selected at the length of the chromosome (feature) and the amount of that gene is mutated. Step 5: Selecting the optimal population according to the fitness function. Checking the termination condition: If not satisfied: Return to step 4 If satisfied: Optimal chromosome declaration

Table 9
The used parameters in classification methods.

Classifier	parameters	Equation
KNN	Euclidean (K=3, K=5, K=7)	$d = \sqrt{\sum_{i=1}^{n}(x_i^1 - x_i^2)^2}$
	Cosine (K=3, K=5, K=7)	$d = 1 - \frac{\sum_{i=1}^{n} x_i^1 x_i^2}{\sqrt{\sum_{i=1}^{n}(x_i^1)^2}\sqrt{\sum_{i=1}^{n}(x_i^2)^2}}$
SVM	Linear	$K(X_i, X_j) = X_i^T X_j$
	Polynomial	$K(X_i, X_j) = (1 + X_i^T X_j)^P$
	Radial basis function (RBF)	$K(X_i, X_j) = \exp(-\frac{\|X_i - X_j\|^2}{2\sigma^2})$
	Gaussian	$K(X_i, X_j) = \tanh(\beta_0 X_i^T X_j + \beta_1)$
MLP	Linear (Purlin)	$n = \sqrt{i + o}$ n: The number of hidden neurons i: number of attributes & o: number of class labels
	Tangent sigmoid (Tansig)	

2.7. Feature normalization

The feature normalization was used to achieve a proper feature set. The feature set was obtained in the new range of $[-1,\ 1]$ by the min-max normalization method.

2.8. Feature selection

After extracting different features of the five different time-series generated from the Poincaré map of RR, QT & ST Intervals, to improve the accuracy of the classification and selection of optimal features, the genetic algorithm method was investigated for this purpose. This method is a bio-inspired algorithm, which can be used to select optimal features. Each gene from a chromosome takes values of zero and one, in which the value of one expresses the existence of attribute in optimal feature space, and the zero value expresses the absence of the attribute. Therefore, the position of a feature in the selected space is coded with zero (non-existence) and one (existence) in binary format. In Table 8, the method of genetic algorithm is briefly presented.

2.9. Feature reduction

Using the genetic algorithm method, optimal features were determined for each of the time series obtained from the Poincaré map of RR, QT & ST Intervals. Thus, to use more important features and to eliminate less important features, and ultimately, to accelerate the process of training the system; the most suitable features must be selected among all the computed features. For this purpose, the P-value criterion was used to further reduce the acquired features space and to select effective more features.

2.10. Classification

After extracting the various features and selecting the most effective features through the genetic algorithm and the P-value criterion, a proper feature set was obtained. Hence, training the classifier was performed to identify emotional states in the two-dimensional model of arousal (high/low) - valence (positive/negative). Different machine learning algorithms have been used to classify human emotional states by providing the features of physiological signals [25].

In this paper, three classification methods including the K-nearest neighbor, support vector machine and multi-layer perceptron neural network were evaluated. In the KNN classifier, a sample of data amongst its k-nearest neighbor is categorized to a certain class that, has several more samples among them [44].

In Table 9, the values of k and two distance is reported for the KNN classifier. Moreover, In Table 9, the samples of x_i^1 and x_i^2 are *ith* feature of first and second classes, respectively. In the SVM method, creating a separator hyper plan has been tried to maximize the distance between the samples of different classes; so the SVM classifier can choose a separator hyper plan with the highest boundary.

There are several functions with the general form: $K(x_i, x_i) \equiv \emptyset(x_i)^T \emptyset(x_i)$ which can be used for classification [45]. In this study, according to Table 9, four different types of kernel functions were used for the SVM classifier. Besides, the number of neurons of the hidden layer and two types of transfer functions are reported for the MLP classifier.

3. Results

The purpose of this study is the analyzing the dynamical behavior of Poincaré map in the form of extraction of the 5 different

time-series from the Poincaré map of RR, QT and ST intervals in the detection of the two-dimensional model of emotion.

In this study, after selecting the appropriate features through the genetic algorithm for each of the time series obtained from RR, QT & ST intervals Poincaré map; and the P-value statistical test were evaluated to distinguish between two classes in the continuous model of emotion for the further reduction of the set of acquired features and selection effective more features. by considering $p < 0.01$ as a significant level, the p-value criterion is obtained for the extracted parameters which are shown in Table 11 (at the end of results section) for the two-dimensional model of AV.

A set of the most appropriate features was classified into two classes of training and testing for each of the time series obtained of Poincaré map; which are reported in Table 11. To the testing data, the k-fold cross-validation technique ($k = 5$) was used.

The simulation results show that for each of the Poincaré maps of the RR, QT & ST intervals; there are distinct optimal features in different domains to identify the emotional state system for the two-class problem.

3.1. The results obtained from the Poincaré map of RR intervals in emotion detection for the two-class problem of arousal (high/low) - valence (positive/negative) model

The results indicate that to identify the system of the emotional state using the nine emotional keywords through electrocardiogram signals, the Poincaré plot of the RR interval time series and appropriate feature set created from the 5 different time-series for the two-class problem of arousal and valence, 19 features and 23 features are extracted as the most suitable features respectively.

These parameters are presented in Table 11 (at the end of the results section). Given that RR intervals are derived from the different sequences of time intervals between successive peaks of R waves in the QRS complex; also this complex are represented the ventricular depolarization; therefore, these intervals are affected for response to the feelings.

The optimal feature extraction in the time domain for the 5 different time-series have represented the variations and dispersion of samples in the time domain, So it can be seen that in the two-dimensional model of emotion, the changes of these parameters are significant for each of the time series extracted from Poincaré map.

Also, for the time series of distance in the polar coordinate it appears that in the DWT with five levels of decomposition according to the morphological of signal, the detail coefficient of d1 and d2 have included one of the waveforms of this time series. The system is almost near stability due to changes from the point of equilibrium and the region of intersection with the 45° line. Due to the existence of high variability, higher frequencies of this time series are more important concerning the decomposition level of the d1 and d2.

Given that obtained entropy from the time series of triangle region in the two-class problem of the AV model, it can be found that the complexity of this time series was significant as a parameter. Also for the system dimension variations, by calculating the correlation dimension, only the dynamics of the time series of the triangle region were significant for both of the levels of arousal and valence.

So using optimal feature extraction, the obtained different time series from Poincaré map of the RR Intervals achieves the best average accuracies of $77.52\,\% \pm 5.84$ and $76.32\,\% \pm 5.47$ in the model of arousal and valence, respectively.

3.2. The results obtained from the Poincaré map of QT Intervals in emotion detection for the two-class problem of arousal (high/low) - valence (positive/negative) model

The results of the Poincaré map of the QT Intervals indicate that for the two-class classification problem of the arousal and valence model; 17 attributes and 22 attributes are selected as the most suitable features of the 5 different time-series, respectively. These parameters are presented in Table 11 (at the end of the results section). Given that the QT intervals are obtained from the sequence of the difference of time intervals between the peak times of two waves of Q & T in each heart cycle, this interval represents the time of ventricular activity; including ventricular depolarization and ventricular repolarization.

This interval is measured from the beginning of the QRS complex to the end of the T wave, and because the value of this interval varies with age and heart rate of the person, so in response to the emotional stimuli, the ventricular activity is undergoing changes that are also influenced on the QT intervals.

In this study, for the features of the time domain, some statistical parameters were significant which were extracted from three-time series including the time series of angle in polar coordinate, the time-series of triangle area created by three consecutive vectors; and the time series of the angle between two successive vectors.

Moreover, for the two-class classification problem of the level of arousal, the obtained mean value from the detail coefficient of d5 of the extracted wavelet transform from the triangle region time series indicates that according to the morphological of signal; d5 has included one of the signal waveforms. Further, it expresses that the lower frequency components of this signal are more valuable; and the amount of complexity of the time series of distance in polar coordinate and the time series disorder of angle between two successive vectors are significant for both of the two-dimensional model of arousal and valence.

The obtained variance parameter from the wavelet transform also indicates the variation and dispersion of the time series of the shortest distance to the 45° line in the time-frequency domain.

Thus, through optimal feature extraction, the obtained different time series from the Poincaré map of the QT intervals achieves the best average accuracies of $79.84\,\% \pm 4.06$ and $77.67\,\% \pm 4.37$ in the arousal and valence model, respectively.

3.3. The results obtained from the Poincaré map of ST intervals in emotion detection for the two-class problem of arousal (high/low) - valence (positive/negative) model

The obtained results of the Poincaré map of the ST Intervals indicate that, in the model of arousal (high/low), 17 features and in the model of valence (positive/negative); 20 features are selected as the most suitable features extracted from the 5 different time-series for the two-class classification problem.

These parameters are presented in Table 11 (at the end of the results section). It should be noted that the time intervals of the waves of Q and S are measured relative to the T waves; so, how of scattering the points in the Poincaré plot of QT and ST intervals shows that it has similar structure and sequence both of them. So most of the extracted parameters from the five different time-series of the Poincaré map of the ST and QT intervals are approximately the same.

Nevertheless, the obtained results from the performance evaluation of classifiers show that the extracted parameters from the different time series generated from the Poincaré map of ST intervals can lead to the better distinction between the two-class problem of AV model in the emotion detection; in comparison with the results obtained from Poincaré map of RR and QT intervals.

Moreover, in compared with the extracted parameters of the different time series generated from the Poincaré map of the RR & QT intervals, the results show that in both of the two-class problem of arousal and valence, the fewer parameters of the different time series generated from the Poincaré map of ST Intervals are achieved.

Since, in the ST interval of the ECG signal; the ST segment is a smooth segment between the end of the S wave and the beginning of the T wave, also it represents the stage of isoelectric in the ECG signal; hence, at this stage, the ventricles are between the stage of depolarization and repolarization.

Therefore, according to the obtained results from this study, for the reason of the high accuracy of the classifier's performance, it can be found that; in response to the emotional stimuli (two-dimensional model of emotion); the ST intervals is more affected than the RR & QT intervals.

So considering the dynamical behavior of the Poincaré map of the ST intervals, the analysis of the obtained time series of this map, the extracted features in the different domain; one can conclude that the stage of between ventricular depolarization and ventricular repolarization will be more affected in response to the emotional stimuli.

On the MAHNOB-HCI dataset, through optimal feature extraction, the different time series generated from the Poincaré map of the ST intervals achieves the best average accuracies of 82.17 % ± 4.73 and 78.07 % ± 3.59 in the arousal and valence model, respectively.

3.4. Assessment of emotion classification based on two-dimensional model of emotion (Arousal-Valence)

Given that the used feature set in the training process of the emotional system includes the selection of the most appropriate features, and all of the different time series generated from Poincaré maps are involved in its formation. Therefore the proper features set are composed with the best emotional information of the different time series obtained from the Poincaré map of different intervals.

In this study, three classifier structures of KNN, SVM, and MLP were used after getting a set of the extracted appropriate features from the different time series of the Poincaré map of RR, QT and ST intervals.

Performance evaluation of the classifiers of KNN, SVM & MLP are reported in Table 10. As mentioned in the previous section, the various parameters used for the classifiers are presented.

By the test data set, the confusion matrix illustrates how of the classification performance by confusion through writing the class problem. The elements make this confusion matrix.

So, that for a two-class problem of AV model; in this study, the first-class belongs to the high arousal or the negative valence and second class belongs to the low arousal or the positive valence; and these elements for each class are:

- True Positive (TP): This criterion indicates that several data are correctly identified in the first class for the arousal dimension (high) or valence dimension (negative).
- True Negative (TN): This criterion indicates that several data are not correctly identified in the second class for the arousal level (low) - or the valence level (positive).
- False Positive (FP): This criterion indicates that several data are identified by mistake in the first class for the arousal level (high) - or the valence level (negative).
- False Negative (FN): This criterion indicates that the number of data is not identified by mistake in the second class for the arousal level (low) - or the valence level (positive).

Eventually, to evaluate the classification results, according to Eqs. (11), (12) and (13), the average accuracy criterion (AVG-ACC), the specificity and sensitivity index was calculated for validating the proposed method. The obtained results from the KNN, MLP & SVM classifiers are presented in Table 10.

$$Accuracy = \frac{TN + TP}{TN + TP + FN + FP} \tag{11}$$

$$Specifity = \frac{TN}{TN + FP} \tag{12}$$

$$Sensitivity = \frac{TP}{TP + FN} \tag{13}$$

4. Discussion

In this study, the focus was on Poincaré mapping of the three-time intervals of RR, QT & ST and extracted different features from the 5-new time series generated in this space. It should be noted that the dynamical behavior analysis of Poincaré mapping of three-time intervals and especially, the extracted parameters from these different time-series of this mapping have yielded significant results.

These parameters extracted from the new different time-series can demonstrate the hidden information of the Poincaré mapping and the hidden behavior of three-time intervals of ECG signals that are affected by emotions. Although the paper results were proximately effective, due to the high computational extensive processing time, it seems that further studies need to done on this research.

For further discussion on the results of this research against the current state of the art, it is discussed in five topics of main findings:

- Extracted 5-different new time series from the Poincaré mapping of the RR, QT & ST Intervals
- Extracted optimal feature set from these new time-series generated in this phase space
- Dynamical behavior analysis of Poincaré mapping points of the RR, QT, & ST Intervals
- Classification and detection of emotions based on the two dimensional AV space of emotions
- Identifying the ST time Intervals as the most effective time intervals of the ECG signal in ANS response to emotional stimuli

Given that, the ST segment representing the isoelectric stage in the ECG signal and at this stage the ventricles are between the depolarization and repolarization stages, the results obtained in this study have shown that this segment is mostly affected in ANS response to emotional stimuli. Therefore, the contribution of knowledge of this research is important to other behavioral and clinical areas. In this study, the results show that the extracted optimal parameters from the new different time-series generated from the Poincaré mapping of the RR, QT & ST time intervals, are well able to show and detect the responses obtained from the arousal (high/low) and valence (positive/negative) dimensions. The combination of features obtained from the new time series generated from Poincaré mapping of time intervals in the domains of time, frequency, time-frequency, and nonlinear analysis are well able to show the dynamical behavior of Poincaré mapping in terms of the two-dimensional model of emotions.

In this study, simple classification methods have used. Each of the three classification methods have disadvantages and advantages that should be considered. KNN classifier can be used as an optimal classification because of its non-dependence on feature space. The SVM classifier operates based on the principle of minimizing experimental error, which this advantage

Table 10
Performance evaluation of the classifiers of KNN, SVM & MLP in the two-class problem of the Arousal-Valence model.

level	Classifiers	The results of extracted features of the 5-different time-series obtained from Poincaré map of RR Intervals			The results of extracted features of the 5-different time-series obtained from Poincaré map of QT Intervals			The results of extracted features of the 5-different time-series obtained from Poincaré map of ST Intervals		
		AVG-ACC (%) ± SD	SPE (%)	SEN (%)	AVG-ACC (%) ± SD	SPE (%)	SEN (%)	AVG-ACC (%) ± SD	SPE (%)	SEN (%)
Arousal level (high/low)	KNN-Euclidean (k = 3)	73.67 ± 0.64	77.07	70.87	77.91 ± 3.08	90.08	71.67	78.29 ± 4.62	84.93	74.03
	KNN-Euclidean (k = 5)	75.19 ± 4.83	83.37	70.43	73.66 ± 5.32	77.1	72.66	80.63 ± 3.41	86.83	76.03
	KNN-Euclidean (k = 7)	76.36 ± 1.79	85.53	72.23	79.84 ± 4.06	87.93	75.6	79.47 ± 2.97	89.57	73.43
	KNN-Cosine (k = 3)	72.48 ± 5.75	80.7	68.07	79.07 ± 2.02	84.33	74.63	77.53 ± 5.46	83.1	73.23
	KNN-Cosine (k = 5)	76.31 ± 6.38	81.93	72.4	75.19 ± 3.57	77.4	73.2	77.13 ± 0.69	84.23	75.73
	KNN-Cosine (k = 7)	75.58 ± 5.29	81.87	71.63	74.43 ± 5.29	81.63	71.7	76.36 ± 4.39	79.57	75.5
	SVM-Linear	74.42 ± 4.65	80.17	70.13	72.87 ± 1.78	75.53	71.6	82.17 ± 4.73	91.97	76.3
	SVM-Polynomial	74.81 ± 4.56	76.9	73.33	77.13 ± 1.79	86.2	72.24	79.46 ± 3.55	81.5	77.93
	SVM-RBF	75.97 ± 4.60	79.83	73.3	74.81 ± 4.37	84.57	70.1	79.84 ± 5.25	84.96	77.06
	SVM- Gaussian	77.52 ± 5.84	85.03	72.8	75.97 ± 5.4	83.1	70.77	80.23 ± 5.08	87.93	75.07
	MLP-Purlin	74.40 ± 5.06	78.67	72.17	77.91 ± 4.17	87.53	72.07	79.07 ± 4.17	85.86	77.3
	MLP-Tansig	75.47 ± 1.15	81.97	72.73	74.03 ± 4.69	81.17	69.9	81.40 ± 4.94	88.67	77.57
Valence level (positive/negative)	KNN-Euclidean (k = 3)	70.61 ± 0.8	75.63	67.47	71.94 ± 5.47	77.9	71	76.77 ± 3.06	86.33	71.53
	KNN-Euclidean (k = 5)	75.47 ± 3.43	87.37	68.97	73.68 ± 4.96	78.57	70.67	76.33 ± 5.2	87.3	70.63
	KNN-Euclidean (k = 7)	71.93 ± 3.64	80.03	68.2	72.37 ± 5.9	79.63	69.4	72.81 ± 4.61	76.63	70.13
	KNN-Cosine (k = 3)	72.83 ± 5.75	82.53	68.83	74.57 ± 2.04	81.93	70.83	73.70 ± 4.5	82.93	68.36
	KNN-Cosine (k = 5)	74.56 ± 4.97	80.83	70.43	74.13 ± 5.96	80.47	71.16	71.50 ± 4.69	74.2	69.56
	KNN-Cosine (k = 7)	73.26 ± 1.98	74.47	73.2	77.67 ± 4.37	86.33	72.47	71.05 ± 5.01	77.2	67.4
	SVM-Linear	75.88 ± 4.18	84.87	70.7	75.00 ± 5.47	80.47	70.77	72.80 ± 3.32	79.03	69
	SVM-Polynomial	76.32 ± 5.47	82.96	71.17	72.82 ± 4.85	81.77	68.53	78.07 ± 3.59	89.63	72.27
	SVM-RBF	71.49 ± 5.06	79.37	67.7	75.87 ± 4.18	81.56	71.87	72.36 ± 6.58	80.93	70.47
	SVM- Gaussian	73.66 ± 1.3	78.87	71.4	75.44 ± 1.98	84	70.93	73.25 ± 1.5	81.9	68.13
	MLP-Purlin	72.37 ± 3.49	79.8	69.9	70.18 ± 3.32	73.93	67.87	74.11 ± 5.3	77.57	72.63
	MLP-Tansig	76.31 ± 4.56	87.37	71.07	73.22 ± 4.62	89.1	66.36	75.90 ± 4.62	81.23	71.77

Table 11
P-value < 0.01 of the extracted features of the 5-different time-series generated from Poincaré maps in the two-class problem of the Arousal-Valence model.

Two-class problem of the level of arousal (high/low)						The two-class problem of the level of valence (positive/negative)					
The extracted features of the 5-different time-series generated from Poincaré map of RR Intervals		The extracted features of the 5-different time-series generated from Poincaré map of QT Intervals		The extracted features of the 5-different time-series generated from Poincaré map of ST Intervals		The extracted features of the 5-different time-series generated from Poincaré map of RR Intervals		The extracted features of the 5-different time-series generated from Poincaré map of QT Intervals		The extracted features of the 5-different time-series generated from Poincaré map of ST Intervals	
Parameters	P < 0.01	Parameters	P < 0.01	Parameters	P < 0.01	Parameters	P < 0.01	Parameters	P < 0.01	Parameters	P < 0.01
Mean (α_I)	4.5696e-04	Max (θ_N)	5.8715e-10	Max (θ_N)	1.5571e-11	Mean (θ_N)	6.6100e-09	Mean (D_N)	3.0396e-06	Max (θ_N)	1.0594e-13
Var (α_I)	2.8624e-04	Var (θ_N)	1.8570e-05	Var (θ_N)	3.2888e-06	Var (θ_N)	5.3138e-07	Max (r_I)	2.1735e-06	Diff_(XI)^2 (θ_N)	4.5595e-06
Diff_(XI)^2 (A_I)	4.6685e-04	Diff_(XI)^2 (A_I)	1.9674e-05	Diff_(XI)^2 (A_I)	3.1878e-05	Var (D_N)	1.0487e-08	Max (θ_N)	1.2377e-13	Diff_(XI)^2 (D_N)	6.3459e-07
Diff_(XI)^2 (A_I)	4.7099e-04	Diff_(XI)^2 (A_I)	1.8968e-06	Diff_(XI)^2 (α_I)	4.7320e-10	Var (A_I)	2.3031e-06	Diff_(XI)^2 (θ_N)	4.5280e-06	Diff_(XI)^2 (A_I)	3.9151e-06
Mean(d1_WT) (r_I)	6.7195e-08	Diff_(XI)^2 (A_I)	3.8874e-05	Diff_(XI)^2 (α_I)	1.9261e-07	Var (α_I)	2.2369e-06	Diff_(XI)^2 (θ_N)	4.5252e-06	Diff_(XI)^2 (A_I)	4.6107e-06
Mean(d2_WT) (r_I)	1.6958e-05	Diff_(XI)^2 (α_I)	6.2384e-12	Diff_(XI)^2 (α_I)	2.0665e-26	Skewness (r_I)	1.6958e-05	Diff_(XI)^2 (D_N)	3.6671e-07	Diff_(XI)^2 (A_I)	4.6267e-07
Mean(d5_WT) (r_I)	2.0449e-04	Diff_(XI)^2 (α_I)	1.3547e-24	Std(d2_WT)(D_N)	3.3584e-06	Skewness (θ_N)	3.2049e-07	Diff_(XI)^2 (A_I)	1.3144e-07	Diff_(XI)^2 (α_I)	8.7411e-06
Mean(a1_WT) (r_I)	6.2686e-21	Mean(d5_WT) (A_I)	1.0620e-05	Mean(d5_WT) (A_I)	1.3494e-05	Diff_(XI)^2 (A_I)	1.3349e-06	Diff_(XI)^2 (A_I)	1.3194e-06	Diff_(XI)^2 (α_I)	4.1219e-06
MAD(d4_WT) (D_N)	4.2969e-04	Hurst (r_I)	1.0737e-09	Hurst (r_I)	5.6503e-10	Diff_(XI)^2 (A_I)	6.6606e-07	Diff_(XI)^2 (α_I)	4.1771e-06	Diff_(XI)^2 (α_I)	1.2085e-15
Std(d3_WT) (A_I)	2.4138e-04	Fuzzy En (α_I)	4.7468e-07	Fuzzy En (α_I)	3.3794e-07	Diff_(XI)^2 (A_I)	2.3879e-06	Diff_(XI)^2 (α_I)	2.1711e-10	Std(a1_WT) (D_N)	8.0617e-07
MAD(d1_WT)(A_I)	1.5318e-04	Coeff$_m$ of AR (θ_N)	2.5981e-09	CD (A_t)	1.2863e-05	RMSSD (A_I)	7.8956e-06	Diff_(XI)^2 (α_I)	8.3944e-17	Hurst (r_I)	1.4894e-09
Mean(d5_WT) (α_I)	2.5858e-06	Coeff$_m$ of AR (D_N)	5.5588e-12	Coeff$_m$ of AR (θ_N)	1.5054e-08	Mean(d2_WT) (r_I)	2.1370e-06	Std(a1_WT) (D_N)	2.3135e-07	Fuzzy En (α_I)	2.0987e-08
Shannon En(A_I)	2.7703e-06	Coeff of AR (r_I)	8.8906e-07	Coeff$_m$ of AR (D_N)	4.7577e-11	Mean(d5_WT)(r_I)	2.3249e-08	Hurst (r_I)	1.0870e-08	Coeff$_m$ of AR (θ_N)	9.3371e-06
Fuzzy En(A_I)	2.4541e-04	Coeff of AR (r_I)	3.8888e-06	Coeff of AR (r_I)	1.8907e-07	Mean(a1_WT) (r_I)	1.8840e-17	Fuzzy En (D_N)	8.6820e-08	Coeff$_m$ of AR (D_N)	5.5710e-07
CD (A_I)	6.0969e-11	Coeff of AR (D_N)	1.8163e-06	Coeff of AR (r_I)	9.0653e-07	Mean(d2_WT) (α_I)	1.0445e-06	Coeff$_m$ of AR (θ_N)	3.3776e-06	Coeff of AR (r_I)	1.5682e-06
Coeff$_m$ of AR (A_I)	1.4799e-09	Coeff of AR (A_I)	4.1766e-05	Coeff of AR (D_N)	5.5631e-06	Mean(d5_WT) (α_I)	2.2516e-06	Coeff$_m$ of AR (D_N)	1.2106e-07	Coeff of AR (r_I)	8.4456e-06
Coeff of AR (r_I)	1.7070e-08	Var of WT (D_N)	1.8188e-06	Var of WT (D_N)	4.3986e-06	MAD(d4_WT) (α_I)	8.3373e-07	Coeff of AR (D_N)	3.8325e-06	Coeff of AR (D_N)	5.4481e-07
Coeff of AR (r_I)	8.2773e-05					CD (A_I)	7.0380e-08	Coeff of AR (D_N)	4.1435e-06	Coeff of AR (D_N)	4.2623e-06
Coeff of AR (A_I)	2.8036e-04					Coeff$_m$ of AR (A_I)	3.7237e-07	Coeff of AR (D_N)	2.9660e-06	Coeff of AR (A_I)	9.1205e-07
						Coeff of AR (A_I)	1.4581e-06	Coeff of AR (A_I)	4.2580e-06	Var of WT (D_N)	4.0539e-11
						Coeff of AR (A_I)	2.2102e-06	Coeff of AR (A_I)	1.4707e-07		
						Coeff of AR (A_I)	2.1784e-06	Var of WT (D_N)	1.8541e-10		
						Coeff of AR (α_I)	5.3739e-09				

Note: Coeff is the abbreviation of Coefficient, and Coeff$_m$ is abbreviation of maximum Coefficient.

Table 12
A comparison of provided methods in the related articles and the proposed algorithm for emotion detection.

Authors	Database	Signals	Emotion	Stimulation	Extracted Parameters	Classifiers	Accuracy
Ben & Lachiri [25]	MAHNOB-HCI	ECG, RESP, SC, GSR	Arousal Valence	Video Clips	Statistical	SVM	64.23 % (A) 68.75 % (V)
Ferdinando et al. [29]	MAHNOB-HCI	ECG	Arousal Valence	Video Clips	Statistical	KNN	59.7 % (A) 55.8 % (V)
Hsu et al. [46]	MAHNOB-HCI	ECG	Arousal Valence	Video Clips	Time Domain, Frequency Domain, Nonlinear Analysis	SFFS-KBCS + GDA + LS-SVM	49.2 % (A) 44.1 % (V)
Ferdinando et al. [47]	MAHNOB-HCI	HRV	Arousal Valence	Video Clips	Time Domain, Frequency Domain, Poincare Analysis	SVM	47.69 % (A) 42.55 % (V)
Anttonen & Surakka [48]	-	HR	Valence	Audio & Visual	Statistical	ANOVA	62.5 % (V)
Jones & Troen [49]	-	BVP, GSR, RESP	Arousal Valence	Pictures	Statistical	neural network	67 % (A) 62 % (V)
Mandryk & Atkins [50]	-	GSR, HR, EMG	Arousal Valence	Computer Game	Statistical	Fuzzy	-
Moharreri et al. [26]	-	HRV	Arousal	Colors	TPSM	Kruskal-Wallis	-
Dabanloo et al. [27]	-	HRV	Valence	Colors	GOM & COM	Kruskal-Wallis	-
Rezaei et al. [28]	-	HRV	Valence	Pictures	Statistical, Frequency Domain, Poincare Analysis	Kruskal-Wallis	-
Subramanian et al. [12]	ASCERTAIN	ECG	Arousal Valence	Video Clips	Statistical	NB + SVM	60 % (A) 59 % (V)
Katsigiannis & Ramzan [14]	DREAMER	ECG	Arousal Valence	Audio & Visual	Statistical	SVM + RBF Kernel	62.37 % (A) 62.37 % (V)
Samara et al. [15]	DEAP	EEG	Arousal Valence	Video	Statistical	SVM	68.15 % (A) 74.53 % (V)
Tzirakis et al. [19]	RECOLA	Speech	Arousal Valence	Audio & Visual	auditory and visual handcrafted	CNN	78 % (A) 73 % (V)
Current Research	MAHNOB-HCI	ECG(use of 5-different time-series generated from ST Intervals Poincaré map)	Arousal Valence	Video Clips	Time Domain, Frequency Domain, Time-Frequency Domain, Nonlinear Domain Analysis	SVM-Linear SVM-Polynomial	82.17 % (A) 78.07 % (V)

results in the improvement of generalization of machine learning. However, they have required complex and time-consuming computational. Test errors may be ignored in the MLP classifier. The generalization of this network is difficult. It is expected that a combination in classification level or advanced-level classification, such as convolution neural network and deep learning, will lead to improve the proposed algorithm classification performance.

Section 4.1 is dedicated to comparisons of the new proposed algorithm results with other literature in the two dimensional model of arousal and valence. In section 4.2, the proposed new algorithm is studied in the field of stress evaluation (stress vs. non-stress). Considering some of the studies that have focused on the distinction between stress and physical activity; It is expected that the proposed new algorithm will be able to distinguish between physical activity and stress using the appropriate feature set extracted from the new different time-series generated from Poincaré mapping of RR, QT, and ST Intervals. Besides, this new algorithm will be able to analyze the phase space dynamic behavior using appropriate feature set extraction from new different time series generated from RR, QT & ST Intervals Poincaré map in the ANS response to stress and physical activity.

4.1. Comparisons of the new proposed algorithm with other existing approaches for MAHNOB-HCI database and other literature

The most optimal feature set was significant with the ability to distinguish between two emotional groups in the continuous model of emotion. Table 11 presents these parameters. From this table, It can be found that one of the extracted features (the features obtained from the different domain analysis) of the five different time-series are capable that have displayed latent information of the Poincaré map in response to the emotional stimuli. In particular, all results have indicated that the extracted features of the 5 different time-series generated from the ST intervals Poincaré map as input parameters for evaluating the classification performance; can provide better results in comparison with the Poincaré map of the RR and QT intervals.

Therefore, the analyzed parameters can recognize; so, these parameters have shown the obtained responses from two emotional groups of high/low for the level of arousal and the positive/negative for the valence level. By the classification of emotional states based on the two-dimensional model of emotion. Table 12 enables a comparison between available methods in the literature and the proposed algorithm.

According to Table 12, in the studies that have used the HRV signal to classify the two-dimensional model of emotion, the performance evaluation of the classification has not reported. In other studies, despite the use of only one signal recorded in different databases, high accuracy was not achieved.

In Table 12, by considering the provided methods of previous studies on the MAHNOB-HCI database, it can be concluded that in the studies that have used different physiological signals and the combination of the extracted features to identify emotion; despite the use of different physiological signals. They have not obtained high accuracy from the emotion detection system, in comparison with other studies that have used a single physiological signal to identify emotion. The results show that the new proposed algorithm can be used as an effective tool for classifying high/low arousal and positive/negative valence via the video clips by using only ECG signals.

Table 13
P-value < 0.01 of the extracted features of the 5-different time-series generated from Poincaré maps in the Stress detection using the WESAD dataset.

Two-class problem of Stress evaluation (stress vs. non-stress)					
The extracted features of the 5-different time-series generated from Poincaré map of RR Intervals		The extracted features of the 5-different time-series generated from Poincaré map of QT Intervals		The extracted features of the 5-different time-series generated from Poincaré map of ST Intervals	
Parameters	P <0.01	Parameters	P <0.01	Parameters	P <0.01
Mean (r_I)	5.0807e-10	Min (θ_N)	7.7803e-09	Min (α_I)	3.9031e-11
Var (A_I)	2.7276e-10	Skewness (A_I)	1.9551e-10	Diff_(XI)^2 (A_I)	7.2609e-09
Skewness (A_I)	8.1168e-11	Diff_(XI)^2 (α_I)	4.2535e-10	Diff_(XI)^2 (α_I)	2.8570e-10
RMSSD (r_I)	6.0831e-10	Diff_(XI)^2 (α_I)	3.9424e-10	Diff_(XI)^2 (α_I)	1.6031e-11
RMSSD (A_I)	1.6179e-09	Max(Diff_(XI)^2) (r_I)	5.9890e-11	Coeff of AR (θ_N)	2.3866e-09
Coeff of AR (D_N)	8.1214e-11	Coeff of AR (D_N)	6.8678e-11	Coeff of AR (D_N)	9.2774e-10
Coeff of AR (A_I)	3.0138e-11				

Note: Coeff is the abbreviation of Coefficient.

Table 14
Performance evaluation of the classifiers of KNN, SVM & MLP in the two-class problem of Stress vs. non-Stress level.

level	Classifiers	The results of extracted features of the 5-different time-series obtained from Poincaré map of RR Intervals			The results of extracted features of the 5-different time-series obtained from Poincaré map of QT Intervals			The results of extracted features of the 5-different time-series obtained from Poincaré map of ST Intervals		
		AVG-ACC (%) ± SD	SPE (%)	SEN (%)	AVG-ACC (%) ± SD	SPE (%)	SEN (%)	AVG-ACC (%) ± SD	SPE (%)	SEN (%)
Stress vs. non-Stress	KNN-Euclidean (k = 3)	83.22 ± 3.30	86.7	82.58	86.70 ± 3.83	88.73	85.81	83.33 ± 5.76	84.45	82.4
	KNN-Euclidean (k = 5)	73.00 ± 4.58	77.28	72.3	85.01 ± 2.95	86.2	84.38	85.83 ± 5.70	94.1	82.13
	KNN-Euclidean (k = 7)	80.83 ± 4.91	82.55	80.1	87.50 ± 5.24	89.98	85.35	80.00 ± 3.07	85.87	79.63
	KNN-Cosine (k = 3)	79.17 ± 5.84	83.95	65.82	83.00 ± 4.21	87.2	81.38	83.33 ± 5.16	84.43	82.8
	KNN-Cosine (k = 5)	75.00 ± 6.05	78.07	74.84	83.40 ± 5.52	86.75	81	84.17 ± 4.92	85.8	75.75
	KNN-Cosine (k = 7)	80.00 ± 5.36	83.78	79.31	84.10 ± 3.76	84.25	84	81.69 ± 2.58	85.4	80.87
	SVM-Linear	85.10 ± 3.16	86.92	84.12	80.83 ± 5.68	87.8	80.8	90.00 ± 5.32	94.73	87
	SVM-Polynomial	75.83 ± 6.83	77.48	75.01	80.00 ± 5.00	80.73	78.27	81.67 ± 4.83	91.12	77.12
	SVM-RBF	78.33 ± 6.63	77.57	76.12	82.00 ± 3.69	89.83	77.03	85.00 ± 3.16	86.12	83.12
	SVM- Gaussian	81.87 ± 2.11	84.86	80.65	82.66 ± 4.94	84.66	80.18	82.50 ± 4.29	87.62	81.95
	MLP-Purlin	82.70 ± 4.52	84.8	82.48	84.20 ± 5.84	90.42	83.45	86.67 ± 5.83	89.19	86.13
	MLP-Tansig	83.40 ± 5.05	83.48	83.3	78.33 ± 4.35	80.92	78.3	83.35 ± 4.74	85.45	82.4

Table 15
Classification performance comparison of the new proposed algorithm for Stress detection.

Authors	Database	Signals	Emotion	Extracted Parameters	Classifiers	Accuracy
Proposed algorithm	WESAD	ECG (use of 5-different time-series generated from ST Intervals Poincaré map)	Stress vs. non-Stress	Time Domain, Frequency Domain, Time-Frequency Domain, Nonlinear Domain Analysis	SVM-linear	90 %
Schmidt et al. [51]	WESAD	ECG	Stress vs. non-Stress	Time Domain, Frequency Domain	LDA	85.44 %

4.2. Comparisons of the new proposed algorithm with other existing approaches for stress evaluation

To extend the new emotion recognition algorithm to other behaviors such as stress evaluation, in this section, by using only the recorded ECG signals in the WESAD dataset, the classification performance of the new proposed algorithm compares with the existing method presented in [51]. Schmidt et al. [51] has developed the WESAD dataset. This dataset is an open dataset for stress and affect detection. Row sensor data was recorded with two devices: a chest-worn device (RespiBAN) and a wrist-worn device (Empatica E4). In this dataset, the ECG, EDA, EMG, TEMP, and RESP signal from the first devices and ACC, BVP, EDA and TEMP signals from the second devices were collected from 15 subjects (12 males and 3 females, age: 27.5 ± 2.4 years). All signals were sampled at 700 Hz.

Based on the affective states of the study protocol [51] (baseline, stress, and amusement condition), in this study, a binary classification task was considered by combining the states of baseline and amusement to a non-stress class, posing the stress vs. non-stress classification problem.

It is important to note that the new proposed emotion detection algorithm can be used as an effective algorithm to detect emotion in the two-dimensional model of emotion. Also in other behaviors including stress evaluation, the new proposed emotion detection algorithm can be used to detect stress for classifying the two-class problem (stress vs. non-stress). The best-extracted feature set is presented in Table 13 that these parameters were extracted from the 5-different time-series generated of the RR, QT and ST intervals Poincaré map. The performance evaluation of the classifiers of KNN, SVM & MLP are reported in Table 14. According to Table 15, in comparison with the study [51], a 5 percent increase in accuracy was obtained. By considering the dynamical behavior of the ST Intervals Poincaré mapping through the 5-different time-series extracted from this mapping in comparison to the Poincaré mapping of QT and RR Intervals, The best classification results are obtained from the ST Intervals Poincaré mapping. Table 15 shows the comparison results, which can indicate that the new proposed algorithm has a better classification performance than a recent study [51]. On the WESAD dataset, through optimal feature extraction of the different time series generated from the Poincaré map of the ST intervals achieves the best average accuracy of 90 % ± 5.23 in the two-class problem classification of stress vs. non-stress level.

Psychological stress causes sympathetic responses in the autonomic nervous system (ANS) [52], therefore, in this study, the

superiority of the obtained results from the extracted features of the five different time-series generated from ST-Intervals Poincaré map expresses that in comparison with RR and QT Intervals, the ST Intervals are more affected by ANS response to stressful stimuli.

5. Conclusion

In this paper, a new emotion detection algorithm presented considering the new time-series generated from the Poincaré map of RR, QT and ST Intervals and genetic algorithm feature selection method, P-value criterion feature reduction and MLP, KNN and SVM classifiers. Only the recorded ECG signals in the MOHNOB-HCI database and WESAD dataset have used for discriminating high/low arousal, positive/negative valence and stress detection (stress vs. non-stress), respectively. The different features extracted from the time domain, frequency domain, time-frequency domain, and nonlinear analysis of the ECG signals to provide discriminative information. The most important results of this study have indicated that the extracted features of the different time-series generated from Poincaré map of RR, QT, and ST intervals were well described in the dynamical behavior of Poincaré map to emotional states detection. It should be noted that in this study, the focus was on the different features extraction from the five different time-series obtained from the Poincaré map of all intervals. The distinct and unique effects of each of the physiological signals in response to emotional stimuli have attracted many researchers in recent years. In the studies of emotion recognition based on ECG Signal, despite the different features extraction such as statistical, frequency and nonlinear analysis, the high accuracy has not been obtained. Moreover, in the studies that have used the HRV signal and the Poincaré map of RR intervals; the hidden information has been ignored in the Poincaré map of the QT and ST intervals.

The results of this study have shown the superiority of the hidden information in the extracted time series from the Poincaré map of the RR, QT, and ST intervals in comparison with the ECG and HRV signals. In many studies, the clinical significance of the ST segment has been studied. The most important finding of this article that can be mentioned is that by considering the superiority of the results that were obtained from the extracted features of different time series generated from the Poincaré map of the ST intervals. It can be concluded that in comparison with the RR and QT intervals; the ST intervals are more influenced in response to the emotional stimuli. The ST Intervals can capture significant changes in ANS response to emotional stimuli.

Introducing these new time-series and feature extracted from them open a new window of research in emotion detection and other behavior e.g. states of sleep monitoring and stress evaluation. This novelty helps researchers to enrich their feature banks to use in different applications.

For future work, each emotion should be considered individually. In the area of feature selection in different domains, linear regression can be used for linearly separable features. The fusion of classifiers level can be used to increase the accuracy, also; the fusion of the extracted optimal features of the different time series generated from Poincaré map of all intervals should be used in emotion detection. Besides, deep learning will be used, so that it has yielded very good results in many studies.

Funding

This research did not receive any specific grant from funding agencies in the public, commercial, or not-for-profit sectors.

Consent for publication

Not applicable.

Ethics approval and consent to participate

This article does not contain any studies with human participants performed by any of the authors.

Availability of data and materials

The data that support the findings of this study are available from [30] but restrictions apply to the availability of these data, which are used under license for the current study, and so are not publicly available. Data are however available from the authors upon reasonable request and with permission of [30]. The datasets analyzed during the current study are available in the MAHNOB-HCI Tagging repository, https://mahnob-db.eu/hci-tagging/ [30].

CRediT authorship contribution statement

MB and KM conceived of the presented idea. MB developed the theory and performed the computations. FF and NJD verified the analytical methods. MB wrote the manuscript with support from KM and FF. All authors provided critical feedback and helped shape the research, analysis, and manuscript. KM supervised the project. All authors read and approved the final manuscript. MB: Writing- Original draft preparation, Software, Validation, Writing-Reviewing and Editing.

Acknowledgments

None.

Declaration of Competing Interest

None declared

References

[1] I.B. Mauss, M.D. Robinson, Measures of emotion: a review, Cogn. Emot. 23 (2009) 209–237, http://dx.doi.org/10.1080/02699930802204677.
[2] E. Fox, Emotion science: cognitive and neuroscientific approaches to understanding human emotions, Choice Rev. Online 46 (2013), http://dx.doi.org/10.5860/choice.46-5903, 46-5903-46-5903.
[3] R. Plutchik, The nature of emotions: human emotions have deep evolutionary roots, a fact that may explain their complexity and provide tools for clinical practice, Am. Sci. 89 (2001) 344–350.
[4] P. Ekman, Ekman_Basic-Emotions.pdf, Handb. Cogn. Emot. (1999) 45–60.
[5] P.J. Lang, The emotion probe: studies of motivation and attention, Am. Psychol. 50 (1995) 372, http://dx.doi.org/10.1037/0003-066X.50.5.372.
[6] J. Posner, J.A. Russell, B.S. Peterson, The circumplex model of affect: an integrative approach to affective neuroscience, cognitive development, and psychopathology, Dev. Psychopathol. 17 (2005) 715–734, http://dx.doi.org/10.1017/S0954579405050340.
[7] K.H. Kim, S.W. Bang, S.R. Kim, Emotion recognition system using short-term monitoring of physiological signals, Med. Biol. Eng. Comput. 42 (2004) 419–427, http://dx.doi.org/10.1007/BF02344719.
[8] J. Kim, E. André, Emotion recognition based on physiological changes in music listening, IEEE Trans. Pattern Anal. Mach. Intell. 30 (2008) 2067–2083, http://dx.doi.org/10.1109/TPAMI.2008.26.
[9] R.W. Picard, E. Vyzas, J. Healey, Toward machine emotional intelligence: analysis of affective physiological state, IEEE Trans. Pattern Anal. Mach. Intell. 23 (2001) 1175–1191, http://dx.doi.org/10.1109/34.954607.
[10] W.-L. Zheng, J.-Y. Zhu, B.-L. Lu, Identifying stable patterns over time for emotion recognition from EEG, IEEE Trans. Affect. Comput. 3045 (2017), http://dx.doi.org/10.1109/TAFFC.2017.2712143, 1–1.
[11] H. Becker, J. Fleureau, P. Guillotel, F. Wendling, I. Merlet, L. Albera, Emotion recognition based on high-resolution EEG recordings and reconstructed brain sources, IEEE Trans. Affect. Comput. 3045 (2017) 1–14, http://dx.doi.org/10.1109/TAFFC.2017.2768030.
[12] R. Subramanian, J. Wache, M.K. Abadi, R.L. Vieriu, S. Winkler, N. Sebe, Ascertain: emotion and personality recognition using commercial sensors, IEEE Trans. Affect. Comput. 9 (2018) 147–160, http://dx.doi.org/10.1109/TAFFC.2016.2625250.
[13] S. Eleftheriadis, O. Rudovic, M. Pantic, Joint facial action unit detection and feature fusion: a multi-conditional learning approach, IEEE Trans. Image Process. 25 (2016) 5727–5742, http://dx.doi.org/10.1109/TIP.2016.2615288.

[14] S. Katsigiannis, N. Ramzan, DREAMER: a database for emotion recognition through EEG and ECG signals from wireless low-cost off-the-shelf devices, IEEE J. Biomed. Health Inf. 22 (2018) 98–107, http://dx.doi.org/10.1109/JBHI.2017.2688239.
[15] A. Samara, M.L.R. Menezes, L. Galway, Feature extraction for emotion recognition and modelling using neurophysiological data, Proc. - 2016 15th Int. Conf. Ubiquitous Comput. Commun. 2016 8th Int. Symp. Cybersp. Secur. IUCC-CSS 2016, 2017, pp. 138–144, http://dx.doi.org/10.1109/IUCC-CSS.2016.027.
[16] S.G. Mangalagowri, P.C.P. Raj, EEG feature extraction and classification using feed forward backpropogation algorithm for emotion detection, 2016 Int. Conf. Electr. Electron. Commun. Comput. Optim. Tech. ICEECCOT 2016 (2017) 183–187, http://dx.doi.org/10.1109/ICEECCOT.2016.7955211.
[17] R. Kar, P. Das, A. Konar, A. Chakraborty, Fuzzy rule enhanced support vector machines for classification of emotions from brain networks, 2nd Int. Conf. Control. Instrumentation, Energy Commun. CIEC 2016 (2016) 153–157, http://dx.doi.org/10.1109/CIEC.2016.7513672.
[18] S. Zhang, S. Zhang, T. Huang, W. Gao, Q. Tian, Learning affective features with a hybrid deep model for audio-visual emotion recognition, IEEE Trans. Circuits Syst. Video Technol. 28 (2018) 3030–3043, http://dx.doi.org/10.1109/TCSVT.2017.2719043.
[19] P. Tzirakis, G. Trigeorgis, M.A. Nicolaou, B.W. Schuller, S. Zafeiriou, End-to-end multimodal emotion recognition using deep neural networks, IEEE J. Sel. Top. Signal Process. 11 (2017) 1301–1309.
[20] J. Perdiz, G. Pires, U.J. Nunes, Emotional state detection based on EMG and EOG biosignals: a short survey, 2017 IEEE 5th Port. Meet. Bioeng. (2017) 1–4, http://dx.doi.org/10.1109/ENBENG.2017.7889451.
[21] K. Michalopoulos, N. Bourbakis, Application of multiscale entropy on EEG signals for emotion detection, 2017 IEEE EMBS Int. Conf. Biomed. Heal. Informatics (2017) 341–344.
[22] P. Gong, H.T. Ma, Y. Wang, Emotion recognition based on the multiple physiological signals, 2016 IEEE Int. Conf. Real-Time Comput. Robot. (2016) 140–143, http://dx.doi.org/10.1109/RCAR.2016.7784015.
[23] W.D. Scherz, R. Seepold, P. Crippa, Distinction of physical activity and stress using RR intervals, (n.d.). https://doi.org/10.15829/1560-4071-2018-10.
[24] W.D. Scherz, R. Seepold, N.M. Madrid, P. Crippa, G. Biagetti, L. Falaschetti, C. Turchetti, Activity monitoring and phase detection using a portable EMG/ECG system, Int. Conf. Appl. Electron. Pervading Ind. Environ. Soc. (2018) 187–194.
[25] M. Ben, Z. Lachiri, Emotion classification in arousal valence model using MAHNOB-HCI database, Int. J. Adv. Comput. Sci. Appl. 8 (2017) 318–323, http://dx.doi.org/10.14569/ijacsa.2017.080344, https://doi.org/10.14569/ijacsa.2017.080344.
[26] S. Moharreri, N.J. Dabanloo, S. Parvaneh, A.M. Nasrabadi, How to interpret psychology from heart rate variability? 2011 1st Middle East Conf. Biomed. Eng. (2011) 296–299, http://dx.doi.org/10.1109/MECBME.2011.5752124.
[27] N.J. Dabanloo, G. Attarodi, S. Moharreri, S. Parvaneh, A.M. Nasrabadi, Emotion recognition based on utilizing occurrence sequence of heart rate's phase space points, IASTED Int. Conf. Biomed. Eng. (2012) 52–55, http://dx.doi.org/10.2316/p.2012.764-116.
[28] S. Rezaei, S. Moharreri, N. Jafarnia Dabanloo, S. Parvaneh, Evaluating valence level of pictures stimuli in heart rate variability response, Comput. Cardiol. 42 (2015) (2010) 1057–1060, http://dx.doi.org/10.1109/CIC.2015.7411096.
[29] H. Ferdinando, T. Seppänen, E. Alasaarela, Comparing features from ECG pattern and HRV analysis for emotion recognition system, 2016 IEEE Conf. Comput. Intell. Bioinforma. Comput. Biol. (2016) 1–6, http://dx.doi.org/10.1109/CIBCB.2016.7758108.
[30] M. Soleymani, J. Lichtenauer, T. Pun, M. Pantic, A multimodal database for affect recognition and implicit tagging, IEEE Trans. Affect. Comput. 3 (2012) 42–55, http://dx.doi.org/10.1109/T-AFFC.2011.25.
[31] G. BegumS, V. Singh, Automatic diagnostic system for long-term ECG data from Holter monitor, Int. J. Comput. Appl. 47 (2012) 16–21, http://dx.doi.org/10.5120/7303-0502.
[32] S.D. Kreibig, Autonomic nervous system activity in emotion: a review, Biol. Psychol. 84 (2010) 394–421, http://dx.doi.org/10.1016/j.biopsycho.2010.03.010.
[33] J. Pan, W.J. Tompkins, A real-time QRS detection algorithm, IEEE Trans. Biomed. Eng. 32 (1985) 230–236, http://dx.doi.org/10.1109/tbme.1985.325532.
[34] A. Page, M. Hassanalieragh, T. Soyata, M.K. Aktas, B. Kantarci, S. Andreescu, Conceptualizing a real-time remote cardiac health monitoring system, in: Med. Imaging Concepts, Methodol. Tools, Appl., IGI Global, 2017, pp. 160–193, http://dx.doi.org/10.4018/978-1-5225-0571-6, ch007.
[35] M.A. Woo, W.G. Stevenson, D.K. Moser, R.B. Trelease, R.M. Harper, Patterns of beat-to-beat heart rate variability in advanced heart failure, Am. Heart J. 123 (1992) 704–710, http://dx.doi.org/10.1016/0002-8703(92)90510-3.
[36] P.W. Kamen, H. Krum, A.M. Tonkin, Poincare plot of heart rate variability allows quantitative display of parasympathetic nervous activity in humans, Clin. Sci. 91 (1996) 201–208.
[37] M.P. Tulppo, T.H. Makikallio, T.E. Takala, T. Seppanen, H.V. Huikuri, Quantitative beat-to-beat analysis of heart rate dynamics during exercise, Am. J. Physiol. Circ. Physiol. 271 (1996) H244–H252.
[38] U.R. Acharya, K.P. Joseph, N. Kannathal, C.M. Lim, J.S. Suri, Heart rate variability: a review, Med. Biol. Eng. Comput. 44 (2006) 1031–1051, http://dx.doi.org/10.1007/978-1-84882-046-3_35.
[39] M.K. Moridani, S.K. Setarehdan, A. Motie Nasrabadi, E. Hajinasrollah, Non-linear feature extraction from HRV signal for mortality prediction of ICU cardiovascular patient, J. Med. Eng. Technol. 40 (2016) 87–98, http://dx.doi.org/10.3109/03091902.2016.1139201.
[40] P. Kaur, P. Bahl, Comparative analysis between DWT and WPD techniques of speech compression, IOSR J. Eng. 2 (2012) 120–128, http://dx.doi.org/10.9790/3021-0281120128.
[41] A. Boardman, F.S. Schlindwein, A.P. Rocha, A study on the optimum order of autoregressive models for heart rate variability, Physiol. Meas. 23 (2002) 325, http://dx.doi.org/10.1088/0967-3334/23/2/308.
[42] T. Gneiting, H. Ševčíková, D.B. Percival, Estimators of fractal dimension: assessing the roughness of time series and spatial data, Stat. Sci. (2012) 247–277, http://dx.doi.org/10.1214/11-STS370.
[43] H. Kantz, T. Schreiber, Nonlinear Time Series Analysis, Cambridge university press, 2004.
[44] P.C. Petrantonakis, L.J. Hadjileontiadis, Emotion recognition from EEG using higher order crossings, IEEE Trans, Inf. Technol. Biomed. 14 (2010) 186–197, http://dx.doi.org/10.1109/TITB.2009.2034649.
[45] C.A. Frantzidis, C. Bratsas, C.L. Papadelis, E. Konstantinidis, C. Pappas, P.D. Bamidis, Toward emotion aware computing: an integrated approach using multichannel neurophysiological recordings and affective visual stimuli, IEEE Trans. Inf. Technol. Biomed. 14 (2010) 589–597, http://dx.doi.org/10.1109/TITB.2010.2041553.
[46] Y.L. Hsu, J.S. Wang, W.C. Chiang, C.H. Hung, Automatic ECG-Based emotion recognition in music listening, IEEE Trans. Affect. Comput. (2017) 1–16, http://dx.doi.org/10.1109/TAFFC.2017.2781732, https://doi.org/10.1109/TAFFC.2017.2781732.
[47] H. Ferdinando, L. Ye, T. Seppänen, E. Alasaarela, Emotion recognition by heart rate variability, Aust. J. Basic Appl. Sci. Aust. J. Basic Appl. Sci. 8 (2014) 50–55.
[48] J. Anttonen, V. Surakka, Emotions and heart rate while sitting on a chair, Proc. SIGCHI Conf. Hum. Factors Comput. Syst. (2005) 491–499, http://dx.doi.org/10.1145/1054972.1055040.
[49] C.M. Jones, T. Troen, Biometric valence and arousal recognition, Proc. 19th Australas. Conf. Comput. Interact. Entertain. User Interfaces (2007) 191–194, http://dx.doi.org/10.1145/1324892.1324929.
[50] R.L. Mandryk, M.S. Atkins, A fuzzy physiological approach for continuously modeling emotion during interaction with play technologies, Int. J. Hum. Stud. 65 (2007) 329–347, http://dx.doi.org/10.1016/j.ijhcs.2006.11.011.
[51] P. Schmidt, A. Reiss, R. Duerichen, K. Van Laerhoven, Introducing WeSAD, a multimodal dataset for wearable stress and affect detection, ICMI 2018 - Proc. 2018 Int. Conf. Multimodal Interact (2018) 400–408, http://dx.doi.org/10.1145/3242969.3242985.
[52] T. Föhr, J. Pietilä, E. Helander, T. Myllymäki, H. Lindholm, H. Rusko, U.M. Kujala, Physical Activity, Body Mass Index and Heart Rate Variability-based Stress and Recovery in 16 275 Finnish Employees: A Cross-sectional Study, 2016, http://dx.doi.org/10.1186/s12889-016-3391-4.